SACLANTCEN REPORT
serial no: SR- 322

SACLANT UNDERSEA RESEARCH CENTRE REPORT

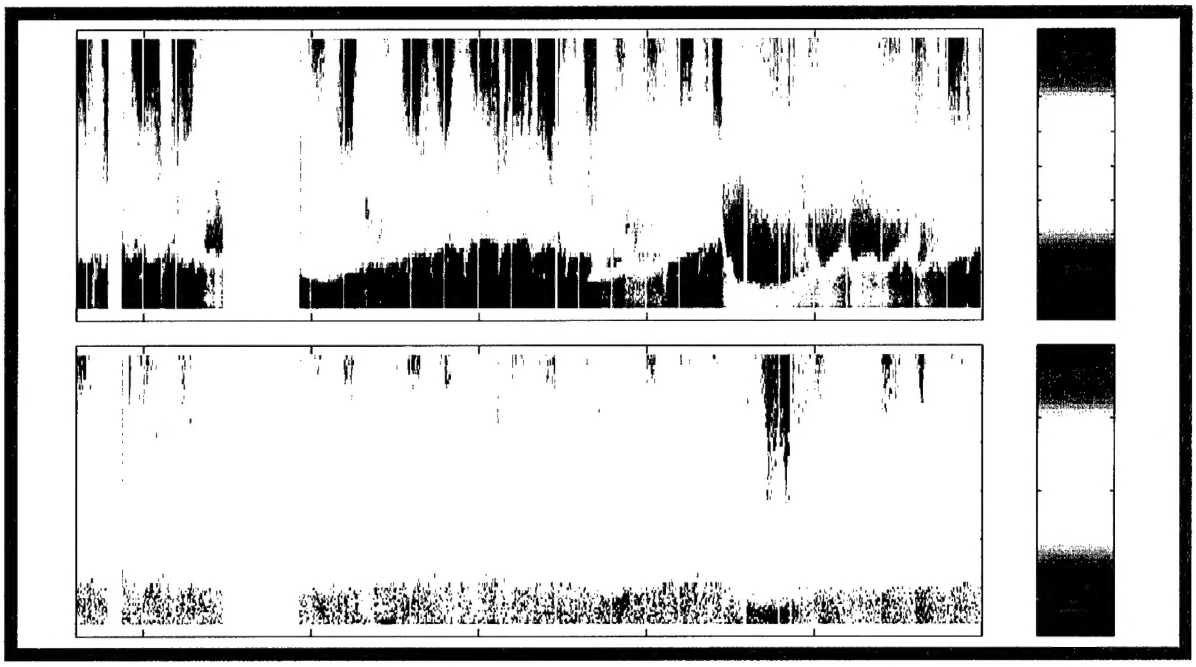

NORTH ATLANTIC TREATY ORGANIZATION ORGANISATION DU TRAITE DE L'ATLANTIQUE NORD

Effects of the atmosphere and sea-surface waves on current and temperature/salinity variations in a shallow water environment.

Daniela Di Iorio, Oddbjorn Bergem and Nicholas Pace

The content of this document pertains to work performed under Project 03-D of the SACLANTCEN Programme of Work. The document has been approved for release by The Director, SACLANTCEN.

Jan L. Spoelstra
Director

intentionally blank page

Effects of the atmosphere and sea-surface waves on current and temperature/salinity variations in a shallow water environment.

Daniela Di Iorio[1], Oddbjorn Bergem and Nicholas Pace

Executive Summary: SACLANTCEN is developing synthetic aperture to provide high spatial resolution for high frequency MCM sonar. A key requisite for synthetic aperture formation is knowledge of the position of the array between sonar transmissions to sub-millimetre accuracy. This need is being addressed by the analysis of the reverberation from the environment following a sonar transmission.

In May/June 1998 an experimental study of acoustic fluctuations in shallow water (10m) was undertaken off the coast of Italy near Carrara. The main objective was to obtain an understanding of processes driven by the atmosphere and by sea-surface waves which might influence the ability to extract the information from reverberation signals required for micro-navigation.

This report is restricted to analysis of only the oceanographic data that were obtained in conjunction with acoustic data. Models of the inter-relationships between pressure, temperature, salinity and sound speed variations during significant changes in ambient conditions are introduced and tested. Such models and results will provide a basis for the study of the limitations imposed by the environment on the techniques of micro-navigation.

[1] Presently at Department of Marine Sciences, University of Georgia, Athens, GA, 30602 (e-mail: daniela@arches.uga.edu)

intentionally blank page

Effects of the atmosphere and sea-surface waves on current and temperature/salinity variations in a shallow water environment.

Daniela Di Iorio, Oddbjorn Bergem and Nicholas Pace

Abstract:

A shallow water experiment ($d = 10$ m) was carried out to measure the contribution of wind, precipitation and sea surface wave effects on current, pressure and temperature/salinity variations. It is found that during heavy rainfall (precipitation exceeding 5 mm), there is a corresponding salinity decrease of approximately 1 psu at 5.8 m depth. Analysis of wind data shows that the cross-shore winds exhibit 24 h periodicity associated with land/sea breezes as a result of land cooling and heating. The 24 h periodicity of cross-shore winds is reflected in temperature and salinity variations leading to the conclusion that advection by wind is the primary cause of low frequency variations. Sea surface wave data show predominantly Mediterranean swell (mean period 4 s and significant wave heights less than 1 m). During the passage of a storm, significant wave heights exceeded 3 m and so the theory of Stokes finite amplitude waves in conjunction with linear theory is used to model particle motion, pressure, temperature/salinity and sound speed variations. Observations and models are compared for six different days and conditions: a local storm event, a calm period, during the peak of a major storm, the post-storm stage, during swell-dominated seas and finally when the sea was calm again. The velocity field shows current oscillations characteristic of a wave boundary layer. The temperature/salinity and hence sound speed variations show that when the orbital particle motions are strong, there is a low frequency spectral power law of $f^{-5/3}$ to the left of the surface wave peak and a high frequency spectral power attenuation of approximately $f^{-3.5}$ to the right.

Keywords: Stokes waves, wave boundary layer, turbulence, Mediterranean Sea

Contents

List of Figures

List of Tables

1

Introduction

The coastal ocean is a highly variable environment. Fresh water inflow, tidal currents, atmospheric forcing, breaking waves are just a few of the features that cause large, low and high frequency variations in temperature, salinity and currents. There is extensive experimental work in the coastal region that focuses on bottom boundary layer dynamics and its influence on sediment transport (Gross et al., 1994) and shallow water wave prediction models for understanding dissipative mechanisms (Shemdin et al., 1978). Our experimental programme was designed to study the influence of atmospheric processes and surface waves on current and temperature/salinity variations in a shallow near-shore location off the west coast of northern Italy.

In this near-shore location, wave boundary layer dynamics dominate over a current boundary layer. This is not the case in many places on the continental shelf or in near-shore locations where wind-driven and tidal currents are of comparable magnitude to wave orbital velocities. Much work has been done to study near-bed orbital wave velocities which in most areas are comparable to near-bed current velocities which leads to wave-current interactions (Grant and Madsen, 1979). Wave velocities are responsible for sediment suspension, transport, ripple formation and geometry. Wave-current interactions lead to high bottom stress. There is an extensive amount of literature available on parameterizing the turbulence in a wave boundary layer and its influence on sediment suspension and transport.

To our knowledge, little work has been done to study the variability of temperature and salinity in a wave boundary layer and hence little is known about mixing rates in this kind of environment. Most work to date is centered on heat flux measurements at the air-sea interface (see for example Edson et al., 1991; Gemmrich and Farmer, 1999). But most of the work is carried out in deep water or in the atmospheric boundary layer.

Linear theory for small amplitude waves is commonly used because much information can be obtained from first order approximations. Second order approximations are required when wave amplitudes become large and when wave breaking occurs (Ippen, 1966). During our experiment a storm caused large sea surface waves providing an opportunity to compare Stokes finite amplitude wave theory and linear theory with observations.

Section 2 describes the experimental configuration. The mean oceanographic variations are described in terms of meteorological conditions in Section 3. Section 4 focuses on the fine scale features of current and temperature/salinity variations and relates them to sea surface wave effects. Conclusions are given in Section 5.

2

Experimental Configuration

A shallow water, acoustic and oceanographic experiment designated *San Gimignano* took place at a depth of 10 m, approximately 800 m cross-shore from the port of Marina di Carrara, which is situated between Genova and Pisa in north Italy (Figure 1(a)). A number of environmental sensors were deployed in order to correlate the effects of oceanographic variability with high frequency acoustic propagation during the period May 23 to June 19, 1998.

Figure 1(b) shows the experimental configuration of acoustic and environmental instruments. A 600 kHz broadband acoustic Doppler current profiler (ADCP) was bottom mounted and cabled to shore so that data could be acquired in real time at a relatively fast sampling rate (Table 1). Periodic sampling was carried out during the experiment and the measurements are used to describe the fine scale velocity variations.

The tower mounted instrumentation comprised a conductivity-temperature-depth (CTD) instrument at 5.8 m depth, cabled to shore for periodic fast sampling (13 Hz), an Aanderaa current meter used only for its conductivity and temperature sensors was at 5.3 m depth sampling mean properties at 10 min intervals and finally a thermistor chain with 11 sensors covering the depth range 2 to 8.5 m mounted to a mast attached to the tower sampling at 10 min intervals.

A directional wave-rider buoy with radio communication to shore operated continuously (with only brief interruptions). Data were acquired for 1600 s at 1.28 Hz

Parameter	Quantity
Frequency, kHz	600
Transmission rate, Hz	2
Ensemble average, transmissions	4
Ensemble interval, s	2
Bin length, m	0.3
Total bins	27
Depth range, m	0.3 to 8.1

Table 1 *Bottom-mounted acoustic Doppler current profiler set up parameters*

sampling and divided into 8 segments of 200 s (256 samples) so that mean quantities describing the surface wave field (significant wave height, mean period, wave height spectrum and directional spectrum for example) were calculated. Results from the 8 segments were then averaged together giving statistics approximately every half hour. Averaging of the spectra within frequency bands of .005 Hz for frequencies $.01 < f < .1$ Hz and bands of .01 Hz for frequencies $.1 < f < .6$ Hz was then carried out. Processing using WAREC (Datawell, 1996) was in real time.

A shore-based meteorological station measured atmospheric conditions every 10 min. Precipitation data were obtained from the meteorological station at Luni airport (approximately 10 km northwest from the Port of Marina di Carrara) and Magra River transport data 12 km north of the river delta was provided by the Servizio Idrografico e Mareografico of Genova.

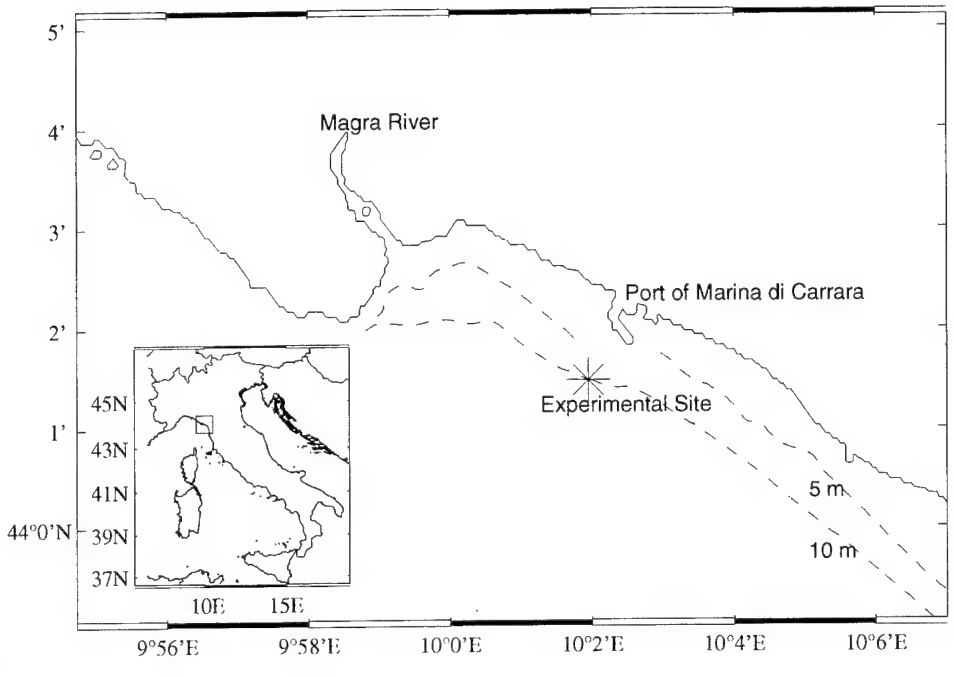

(a)

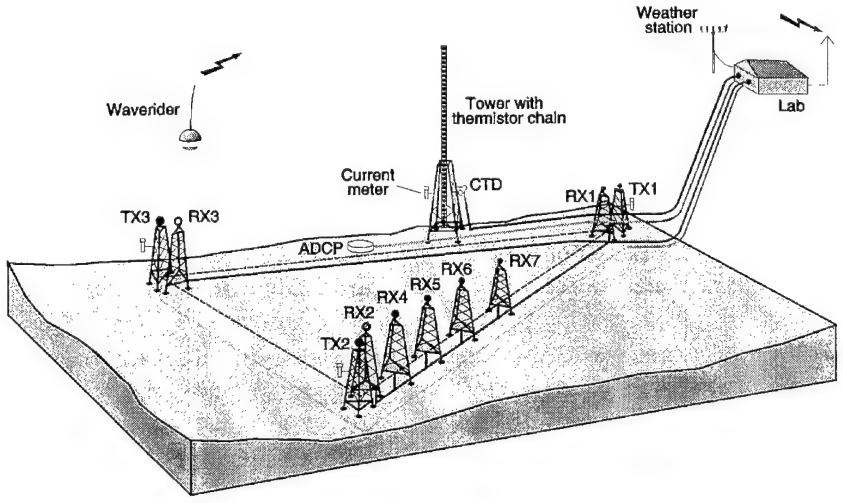

(b)

Figure 1 *(a) Experiment location. (b) Instrumentation configuration during the San Gimignano experiment.*

3

Low frequency variations

Daily averaged Magra river transport measurements for 1997 and 1998 are shown in Figure 2. Increased levels are associated with winter rainfall and snow melt during April/May. The experimental period is from May 23 to June 19, 1998 when the river outflow is approximately 15 m^3 s^{-1}.

Figure 3 shows the mean cross-shore and alongshore currents at 5.4 m measured from the bottom mounted ADCP. The typical averaging interval is 20 min. The only significant currents are alongshore to the northwest. The figure also shows temperature, conductivity and salinity measurements from the moored current meter at 5.3 m depth, precipitation and transport levels. The temperature shows a heating trend. More detailed temperature variability will be analyzed using thermistor chain data. The conductivity sensor was subject to biological fouling. On Year Day 156.424 (Jun. 5 at 1010 UTC) the sensor was cleaned. The dotted curve shows the measured levels and the solid curve shows an assumed corrected conductivity by removing a linear relation from the start of the measurement so that the discontinuity after cleaning is removed. (The current meter was deployed on Year Day 132 and thus there is a difference in measured and corrected levels at the start of the figure.) This same linear relation was applied to the data obtained after cleaning, assuming that biological fouling occurs at a constant rate over this time interval. The salinity was recalculated with corrected conductivity. The salinity from the measured conductivity is shown as a dotted curve and the salinity from the corrected conductivity is shown as a solid curve.

The salinity time series shows variability that could be directly related to the fresh water input by precipitation. When there was rainfall, the Magra River transport shows an increase in level of the order 10 m^3 s^{-1} and the salinity shows a decrease of the order 0.5-1 psu. As the experimental site was 800 m from shore and approximately 2 km from the Magra river mouth, runoff from the shore, river and storm drains could cause the observed salinity decrease. However, on Year Day 168 large changes exist that do not correspond to fresh water input. Advection because of wind could result in variations over a 24 h time scale as will be discussed.

Atmospheric and surface wave conditions are summarized in Figure 4(a). Mean winds of the order 5 m s^{-1} prevailed except during storm conditions when the winds were 10 m s^{-1} or more. The air temperature shows diurnal changes associated with

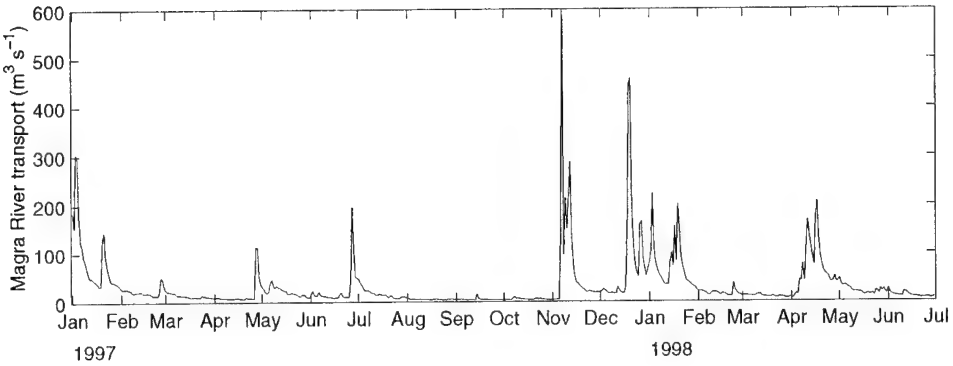

Figure 2 *Daily averaged Magra River transport measurements over a period of 1.5 years.*

land heating and cooling. The air pressure shows low pressure values during storm events. The mean period and significant wave height for the sea surface waves shows an average wave period of 4 s (which corresponds to Mediterranean swell) except during the storm on Year day 162 when wave periods reached 7 s. Significant wave heights were typically less than 1 m except during the storm when heights exceeded 3 m.

The wind velocity data were classified as alongshore (300^oT) and cross-shore (30^oT) components, the power spectrum for each component is shown in Figure 4(b). The power spectrum for the cross-shore winds has been arbitrarily scaled vertically by a factor of 5. The cross-shore winds show strong periodicity of 24 hours. During the day, when the land was warming, winds were primarily from the southwest (a sea breeze). At night as the land cooled, winds were primarily from the northeast (a land breeze). The power spectrum for the alongshore winds do not show a 24 h periodicity, however the 12 h harmonic is present in both spectra with higher levels in the alongshore spectrum.

The mean temperature variability from the thermistor chain data is shown in Figure 5(a). Time series are plotted at each depth. The near surface sensor undergoes the greatest variability and variations in temperature can be traced to the deeper sensors. The temperature power spectra for specific depths are shown in Figure 5(b). The dominant period in the temperature variability is 24 h which corresponds to the periodicity of the cross-shore winds. The greatest 24 h, periodicity occurs at the near surface, attenuating with depth. The 12 h harmonic can be identified for the near surface measurements. Tides in this area are less than 50 cm and the tidal constituents do not show up in the spectra. Thus it is the wind that causes the large low frequency changes in temperature and presumably affects the salinity as well. We can assume that the winds create onshore/offshore surface currents that advect warm water back and forth thus creating up/downwelling conditions.

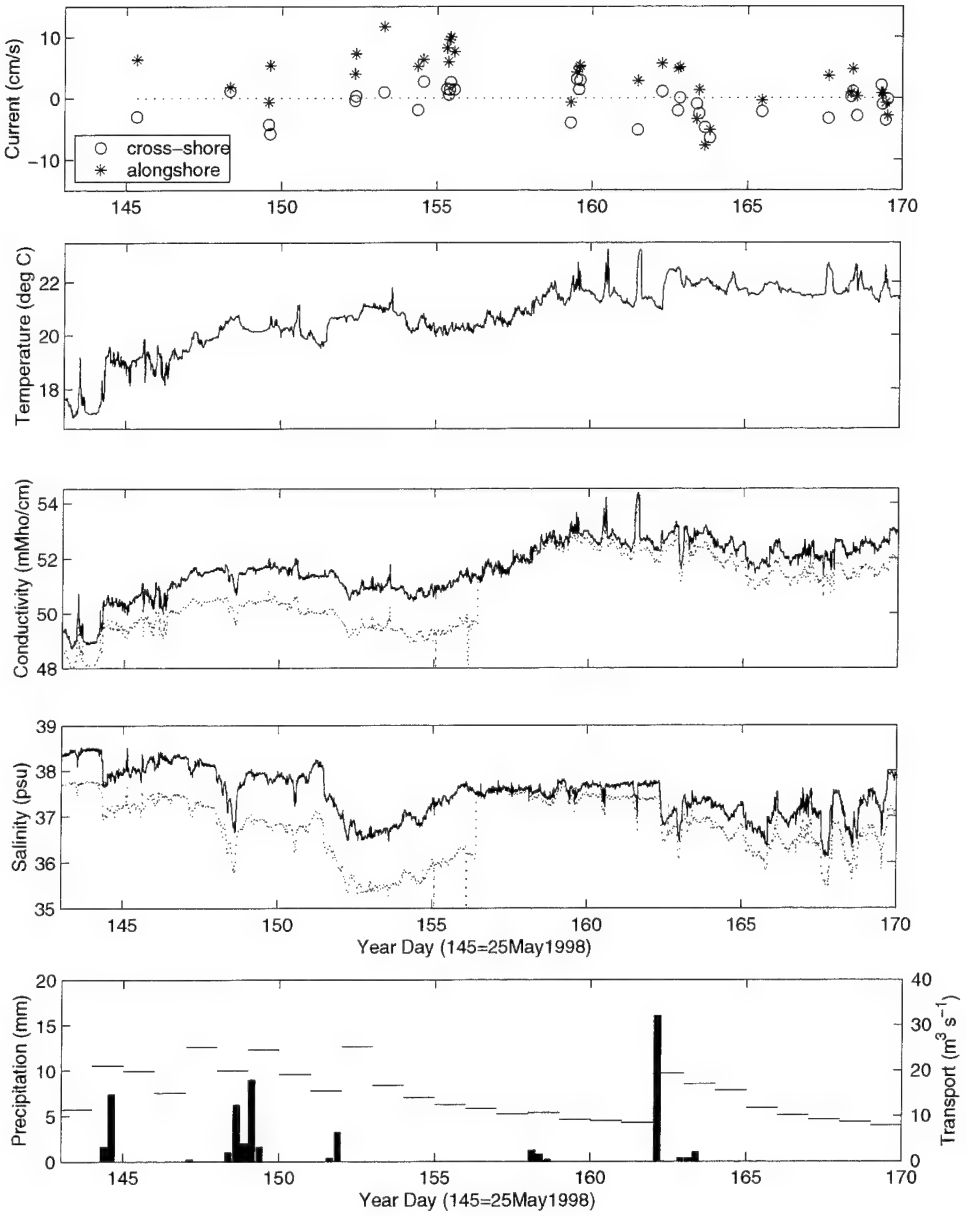

Figure 3 *The mean cross-shore and alongshore current at 5.4 m depth measured from the ADCP. Temperature, conductivity and salinity measured from the Aanderaa current meter moored at 5.3 m depth. The effects of biofouling (dotted curve) have been assumed corrected in the solid curve. Precipitation measured at Luni airport (bar graph) with daily averaged Magra River transport measured at station Calamazza (long dash curve).*

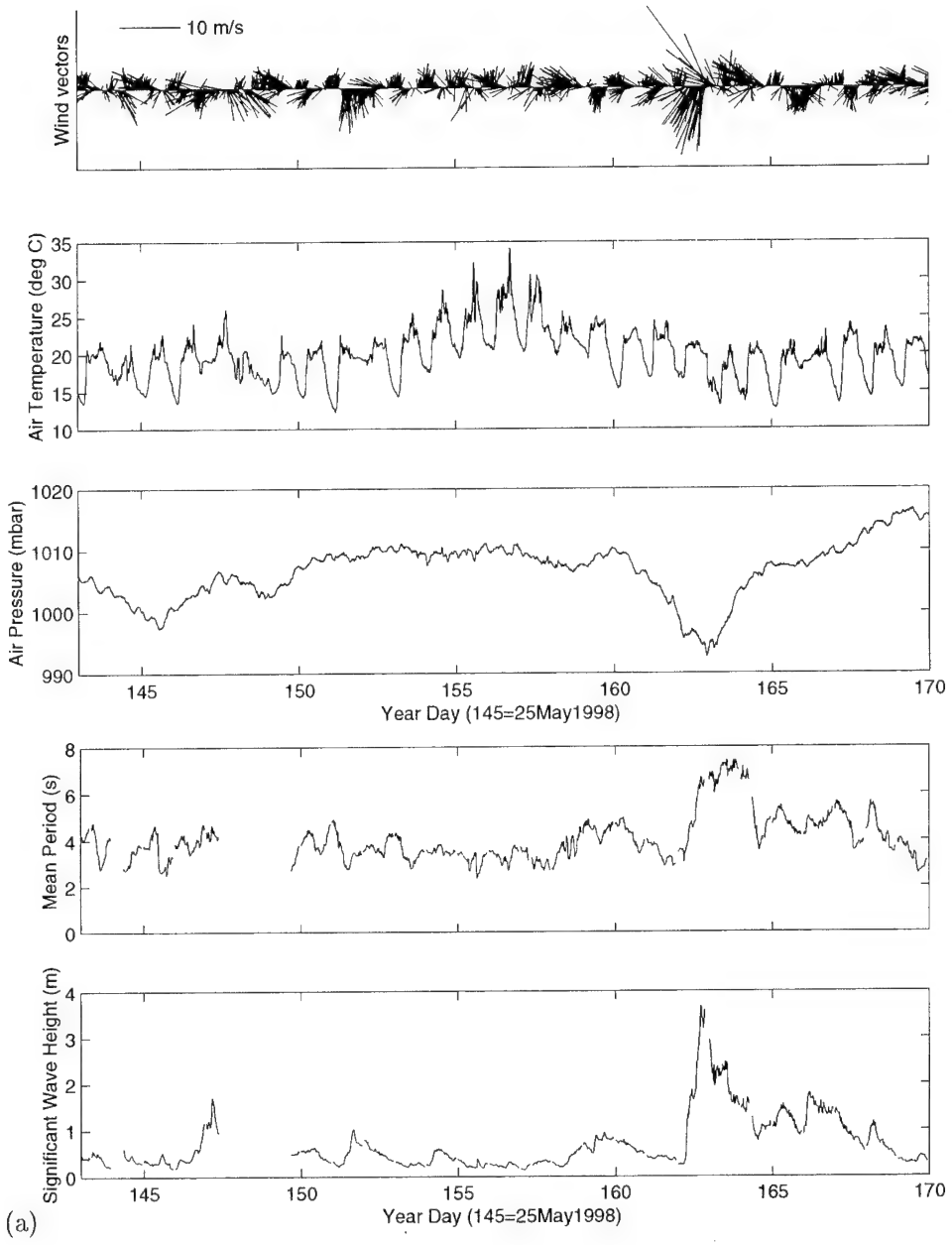

Figure 4 *(a) Meteorological data showing wind vectors, air temperature and air pressure. The mean period and significant wave height measured from the directional wave rider buoy. (b) Power spectrum of the cross-shore (30 °T) and alongshore (300 °T) components of the wind. The cross-shore component has been arbitrarily scaled vertically by a factor of 5.*

(b)

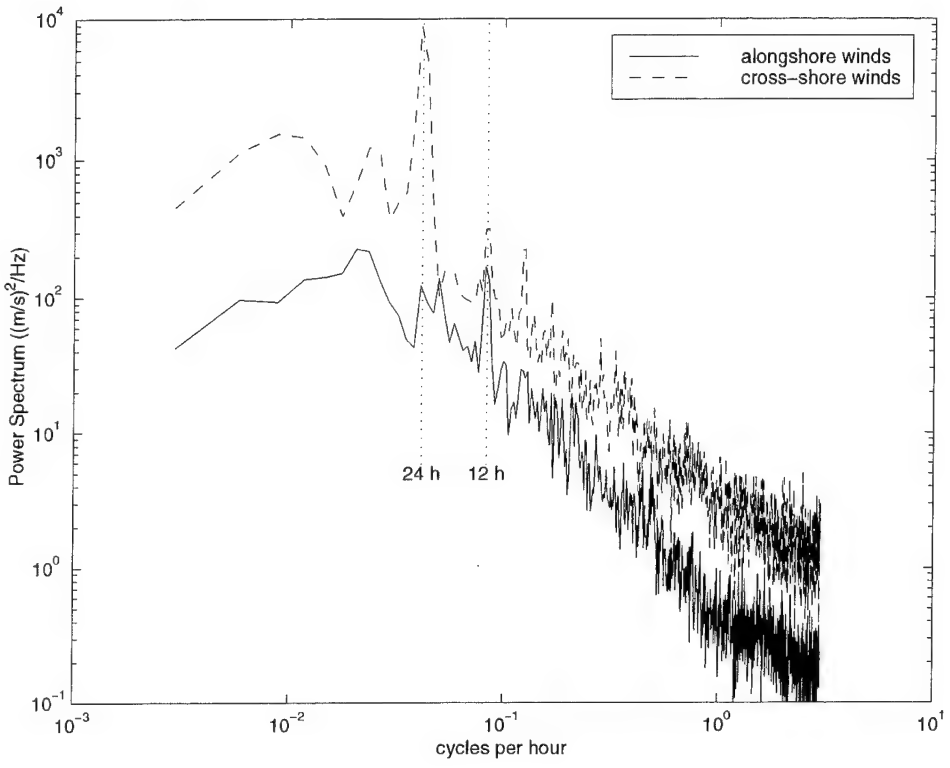

Figure 4 *(continued).*

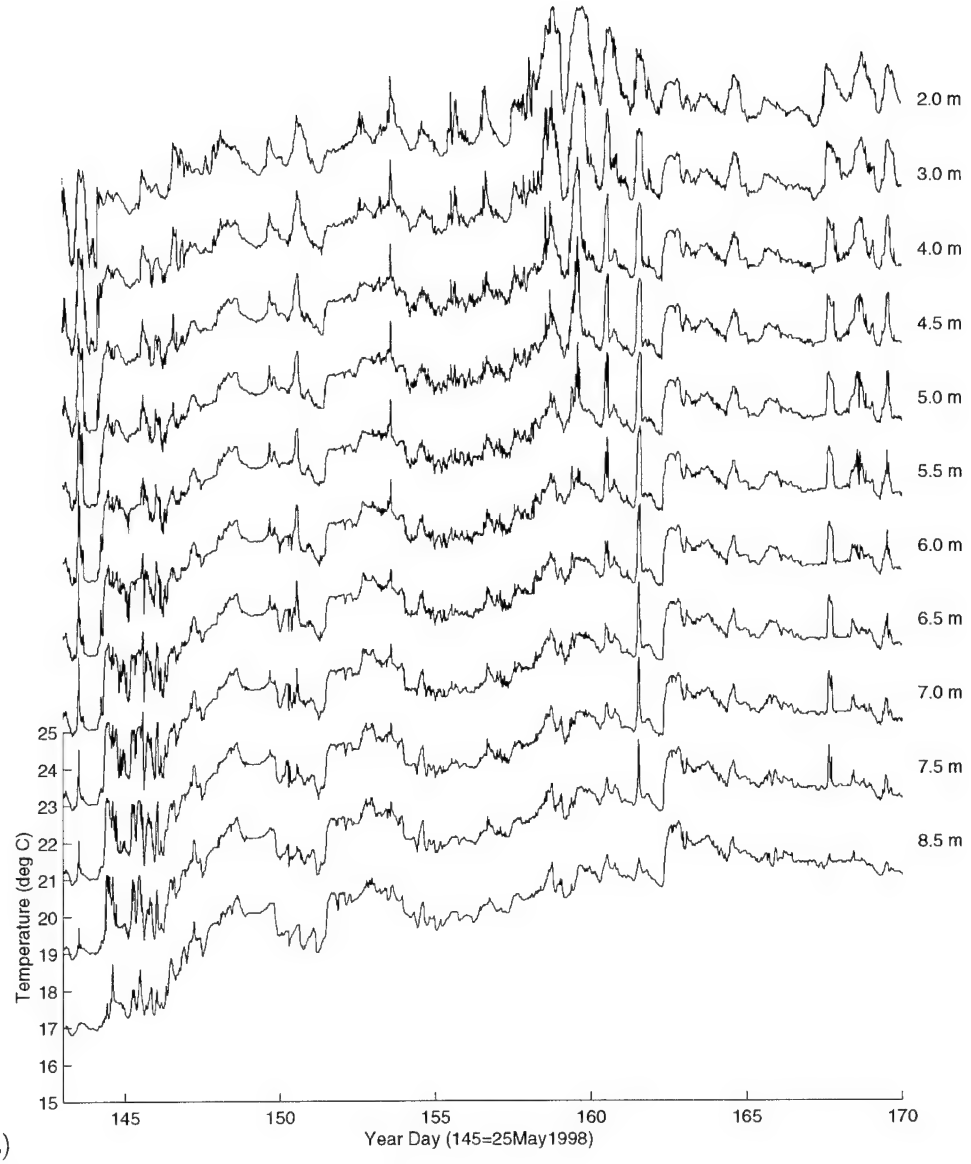

(a)

Figure 5 *(a) Thermistor chain time series data for all sensors and (b) the temperature power spectral density for certain depths, scaled by a factor of 10 relative to the 8.5 m spectrum.*

(b)

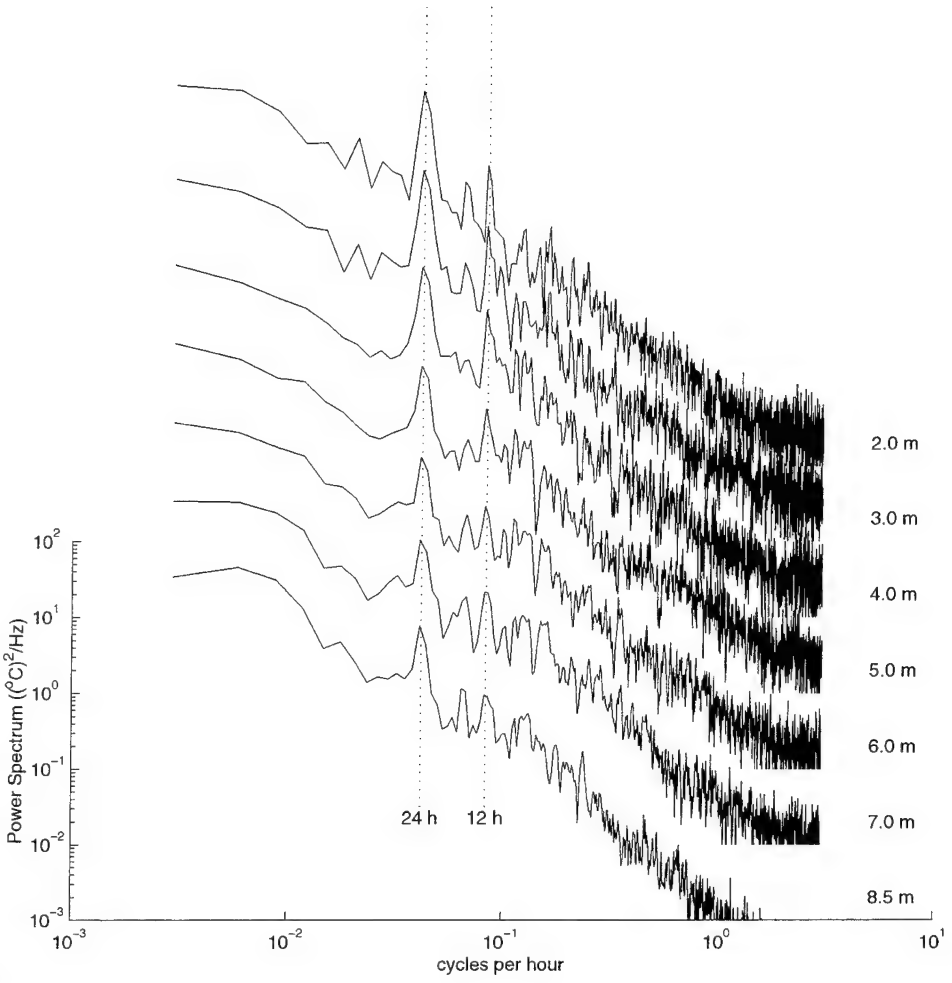

Figure 5 *(continued).*

4

Surface wave effects

In the following section we present some of the theoretical aspects of surface waves of finite amplitude in shallow water ($d = 10$ m). It is expected that the significant surface wavelengths (L) will vary from 20 to 100 m such that the relative depth (d/L) is less than one, thus invoking shallow water theory. As the wave amplitude (a) increases during the storm (Figure 4) the relative height (a/L) and the ratio of wave height to water depth (a/d) become important (Ippen, 1966). Thus we make use of Stokes theory which solves the equations of motion using perturbation methods. The following solutions presented are then to second order.

Since we are dealing with wave spectra we invoke linear theory (Bowden, 1983) to represent the sea surface elevation, particle motion and displacement as a linear summation over all wave components present. Each component is to second order and has its own characteristic amplitude, wavenumber, angular frequency and random phase.

4.1 Theoretical background

Bernoulli's equation for unsteady flow assuming continuity, irrotation and constant density (Lamb, 1932) is,

$$p = -\rho g z + \rho \frac{\partial \Phi}{\partial t} - \frac{\rho}{2}\left[\left(\frac{\partial \Phi}{\partial x}\right)^2 + \left(\frac{\partial \Phi}{\partial z}\right)^2\right], \tag{1}$$

where p is the pressure at depth z which is positive upwards, ρ is the mean density assumed to be independent of time and space, g is gravity and Φ is the velocity potential defined such that the particle motion $u = -\partial\Phi/\partial x$ and $w = -\partial\Phi/\partial z$. The dynamic boundary condition which applies at the free surface $z = \zeta_o$ is,

$$p_a = -\rho g \zeta_o + \rho \left.\frac{\partial \Phi}{\partial t}\right|_{z=\zeta_o} - \frac{\rho}{2}\left[\left(\frac{\partial \Phi}{\partial x}\right)^2 + \left(\frac{\partial \Phi}{\partial z}\right)^2\right]_{z=\zeta_o} = \text{constant}. \tag{2}$$

where p_a is the atmospheric pressure.

For two-dimensional finite amplitude waves in shallow water of depth $z = -d$, nonlinear terms are retained to second order as described by Ippen (1966). The

following equations for the n^{th} harmonic are obtained for the dispersion relation, velocity potential Φ_n and surface wave height ζ_{on} for a particular angular frequency ω_n and wavenumber k_n,

$$\omega_n^2 = g k_n \tanh k_n d, \tag{3}$$

$$\begin{aligned}\Phi_n &= -a_n c_n \frac{\cosh k_n(z+d)}{\sinh k_n d} \sin(k_n x - \omega_n t + \phi_n) \\ &\quad -\frac{3}{8} a_n^2 c_n k_n \frac{\cosh 2k_n(z+d)}{(\sinh k_n d)^4} \sin 2(k_n x - \omega_n t + \phi_n),\end{aligned} \tag{4}$$

$$\begin{aligned}\zeta_{on} &= a_n \cos(k_n x - \omega_n t + \phi_n) \\ &\quad +\frac{1}{4} a_n^2 k_n \frac{(2+\cosh 2k_n d)\cosh k_n d}{(\sinh k_n d)^3} \cos 2(k_n x - \omega_n t + \phi_n),\end{aligned} \tag{5}$$

with kinematic boundary condition for the vertical particle velocity,

$$w = \begin{cases} \frac{\partial \zeta_o}{\partial t} + u \frac{\partial \zeta_o}{\partial x} & \text{for } z = \zeta_o \\ 0 & \text{for } z = -d \end{cases} . \tag{6}$$

According to Neumann and Pierson (1966), obtaining functions ζ_o and Φ which satisfy all the boundary conditions (2) and (6) identically has never been done and probably will never be done as the equations are nonlinear. However, approximations have been derived and are quoted in the literature.

From the velocity potential, the horizontal u_n particle motion is

$$\begin{aligned}u_n &= a_n \omega_n \frac{\cosh k_n(z+d)}{\sinh k_n d} \cos(k_n x - \omega_n t + \phi_n) + \\ &\quad \frac{3}{4} a_n^2 \omega_n k_n \frac{\cosh 2k_n(z+d)}{(\sinh k_n d)^4} \cos 2(k_n x - \omega_n t + \phi_n).\end{aligned} \tag{7}$$

The vertical particle displacement can be approximated by (Ippen, 1966),

$$\begin{aligned}\zeta_n &= a_n \frac{\sinh k_n(z+d)}{\sinh k_n d} \cos(k_n x - \omega_n t + \phi_n) + \frac{1}{4} a_n^2 k_n \frac{\sinh 2k_n(z+d)}{(\sinh k_n d)^2} \\ &\quad +\frac{3}{8} a_n^2 k_n \frac{\sinh 2k_n(z+d)}{(\sinh k_n d)^4} \cos 2(k_n x - \omega_n t + \phi_n).\end{aligned} \tag{8}$$

From Bernoulli's equation (1) the pressure change from hydrostatic equilibrium as a result of the n^{th} harmonic surface wave is,

$$\begin{aligned}\delta p_n &= \rho g a_n \frac{\cosh k_n(z+d)}{\cosh k_n d} \cos(k_n x - \omega_n t + \phi_n) - \frac{1}{4} \rho a_n^2 \omega_n^2 \frac{\cosh 2k_n(z+d)}{(\sinh k_n d)^2} \\ &\quad +\frac{1}{4} \frac{\rho a_n^2 \omega_n^2}{(\sinh k_n d)^2} \left[\frac{3\cosh 2k_n(z+d)}{(\sinh k_n d)^2} - 1 \right] \cos 2(k_n x - \omega_n t + \phi_n).\end{aligned} \tag{9}$$

The angle ϕ_n in all equations is a random phase lag between 0 and 2π and represents that the source of the wave with angular frequency ω_n and wavenumber k_n originates at a different location and time.

The resulting expressions then hold for the sea surface height, vertical displacement, horizontal particle velocity and pressure assuming a spectrum of wave motions,

$$\zeta_o(x,t) = \sum_{n=1}^{\infty} \zeta_{on}(x,t), \tag{10}$$

$$\zeta(x,z,t) = \sum_{n=1}^{\infty} \zeta_n(x,z,t), \tag{11}$$

$$u(x,z,t) = \sum_{n=1}^{\infty} u_n(x,z,t)\cos(\beta - \alpha(f_n)), \tag{12}$$

$$p(x,z,t) = -\rho g z + \sum_{n=1}^{\infty} \delta p_n(x,z,t), \tag{13}$$

where $\alpha(f_n)$ is the directional frequency spectrum and $\beta = 30^o T$ is a fixed angle so that u becomes the cross-shore orbital velocity component.

The amplitude of the n^{th} harmonic is determined from the power spectrum $S(f_n)$ for the wave height since,

$$\sum_{n=1}^{\infty} <\zeta_{on}^2> = \sum_{n=1}^{\infty} S(f_n)\Delta f = <{\zeta_o}^2> . \tag{14}$$

Therefore the amplitude a_n^2 can be found from the quadratic equation,

$$\frac{A_n^2 k_n^2}{32} a_n^4 + \frac{1}{2} a_n^2 - S(f_n)\Delta f = 0, \tag{15}$$

where

$$A_n = \frac{(2 + \cosh 2k_n d)\cosh k_n d}{(\sinh k_n d)^3}, \tag{16}$$

$$\Delta f = \begin{cases} .005\ Hz & 0.01 < f_n < 0.1\ Hz \\ .0075\ Hz & f_n = 0.1\ Hz \\ .01\ Hz & 0.1 < f_n < 0.6\ Hz \end{cases} . \tag{17}$$

The temperature and salinity variations are modelled as a result of the vertical displacement of water particles in the presence of stratification assuming that the water masses are homogeneous in the horizontal over the scales of the horizontal displacement. In shallow water the horizontal scales are typically much larger than the vertical scales and so,

$$T' = \zeta \frac{\partial T}{\partial z}, \tag{18}$$

$$S' = \zeta \frac{\partial S}{\partial z}. \tag{19}$$

Density is dependent primarily on the salinity variations and the sound speed variations are dependent on temperature, salinity and pressure. Since the field study involved acoustic propagation measurements, an analysis of sound speed variations is also given. Soundspeed fluctuations can also be modelled as

$$c' = \zeta \frac{\partial c}{\partial z}. \tag{20}$$

For small changes in the sound speed, the gradient can be expressed in terms of temperature and salinity gradients as,

$$\frac{1}{c_o}\frac{dc}{dz} = a\frac{\partial T}{\partial z} + b\frac{\partial S}{\partial z}, \tag{21}$$

where $a = 1.7 \times 10^{-3}$ $(^{\circ}\mathrm{C})^{-1}$ and $b = 0.73 \times 10^{-3}$ $(\mathrm{psu})^{-1}$ are coefficients determined specifically for this shallow water environment.

4.2 Observations

The power spectral density for the sea surface wave height and the directional spectra are shown in Figure 6. Sample spectra on the left correspond to the evolution of the storm as the wind speed increases from 6.3 to 11.4 m s^{-1} on Year Day 162. As the wind speed increases the spectral peak decreases in frequency and increases in magnitude. The high frequency attenuation follows a f^{-4} power law consistent with Phillips (1985) and Donelan et al. (1985) for wind-generated waves. Most of the waves propagate from the direction 200 to $300^{o}T$ as the sample plot shows. The red areas of the surface wave power density indicate that the significant wave height approaches or exceeds 1 m. The major storm event on Year Day 162 lasts for almost two days and large swell-dominated post-storm conditions continue for approximately four days after the storm.

The amplitude for the n^{th} harmonic wave is calculated from (15) using the wave power density at frequency f_n and the wavenumber k_n calculated from the dispersion relation (3). The amplitude a_n, angular frequency ω_n and wavenumber k_n are used to model the orbital motion, pressure and sound speed, to explain the fine scale variability on Year Day 159.49 (a local storm), 161.43 (a calm period), 162.73 (major storm peak), 163.34 (post-storm stage), 168.32 (swell-dominated sea) and Year Day 169.30 (calm again).

From the bottom mounted ADCP the cross-shore and alongshore current components were calculated (resolved along $30^{o}T$ and $120^{o}T$ respectively). Typically, ADCP measurements were made for 20 min on selected days. It transpired that during the 20 min data collection, the 2 s sampling interval was not always constant. There were periods when there were gaps of 4 and 8 s. The loss of data was presumably associated with the time required to write the data to disk.

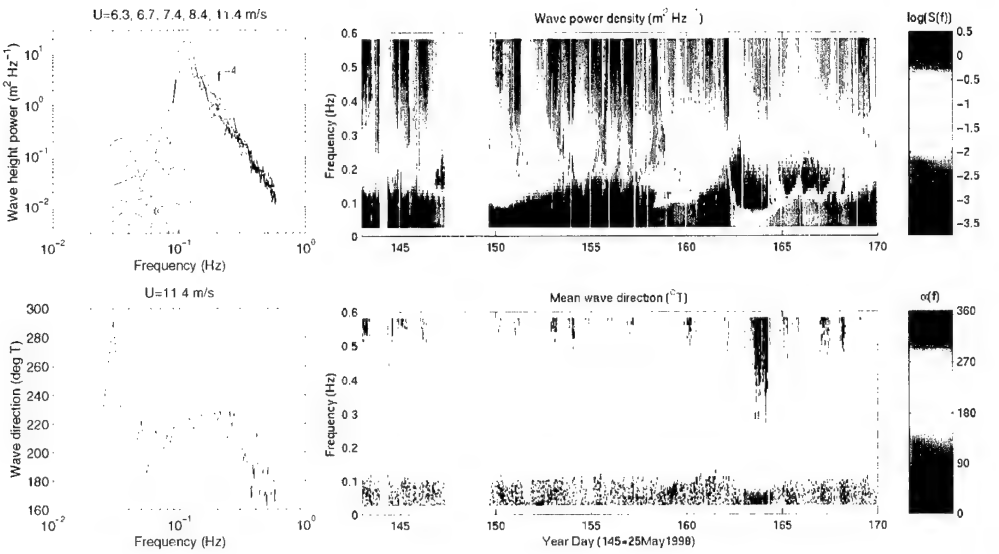

Figure 6 *The power spectral density of the sea surface wave height as a function of frequency and time and the mean direction of the surface waves as a function of frequency and time. Sample spectra during the onset of the storm show a f^{-4} dependency with a mean wave direction of 220 ^oT.*

Figure 7 shows an example of velocity profiles on Year day 163.34 during the storm. The three solid-line profiles correspond in time to half a wave period (4 s) and show an oscillatory wave boundary layer. The dashed curve represents the mean profile averaged over 20 min of data. The observed wave current magnitude is greater than wind-driven or tidal currents for this area as the mean profile is less than the orbital motion. Mean currents (Figure 3) seldom exceeded 10 cm s^{-1}. Based on this result and observations from other days when significant wave heights exceeded 0.5 m, it is concluded that wave advection would be the primary cause for turbulent velocity. The most widely used relationship between orbital velocity and turbulence (see Wiberg, 1995) is the wave Reynolds number,

$$\mathrm{Re} = \frac{U_{om}^2}{\omega\nu}, \tag{22}$$

where U_{om} is the maximum orbital velocity, ω is the orbital wave frequency and ν is kinematic viscosity. For the storm event shown in Figure 7 the wave Reynolds number is 3.4×10^6 which corresponds to fully developed turbulent medium.

As the current velocity shows oscillations indicative of sea surface wave effects, linear interpolation between the 4 and 8 s gaps was not an option and thus the Lomb periodogram described in Press et al. (1986) for unevenly sampled data was carried out for spectral analysis. The results are shown as dotted line curves in Figure 8 for six different days with model results as dashed curves. The modelled results

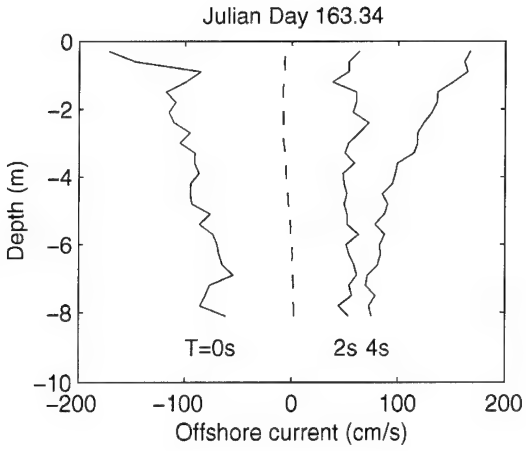

Figure 7 *Velocity profiles in an oscillatory boundary layer over a half wave period at the peak of the storm. The mean profile over 10 min is shown as a dashed curve.*

for the cross-shore orbital motion follows from generating a time series of $u(x = 0, z = -5.7m, t)$ sampled at the same rate as the wave rider buoy (1.28 Hz) and then computing the power spectrum.

On Year Day 159.49 significant wave heights approached 1 m and the wave height spectrum showed two dominant peaks. These peaks are reproduced in the measured and modelled cross-shore current power spectra. The low frequency peak may be associated with incoming swell and the higher frequency peak may be the result of local wind effects. On Year Days 161.43 (prior to the storm) and 169.30 (once the swell-dominated seas subsided) the surface wave heights were characteristic of calm conditions and thus the orbital motion was within the noise of the ADCP measurement. The noise level from the spectra is centred at 5×10^{-3} m^2 s^{-2} Hz^{-1} and the computed root-mean-square (rms) velocity sensitivity is 7.5×10^{-2} m s^{-1}. On other days the orbital motion spectral peak was higher than the noise level and therefore the effects of the surface waves are seen. The comparison between modelled and measured is good, as the spectral peak identified in the model shows up in the measurement. However, during the storm (Year Day 162.73 and 163.34) the modelled spectral peak levels are significantly greater than the observed levels. As the storm passes the spectral level decreases and the peak shifts toward higher frequencies.

Because of the limitations of the ADCP measurement, the fine scale current variations associated with turbulence cannot be seen. Lumley and Terray (1983) present a theory describing the frequency spectrum for turbulent velocity within a wave boundary layer. Measurements by Gross et al. (1994) show that for frequencies greater than the orbital motions, the spectra exhibit a $-5/3$ slope leading to es-

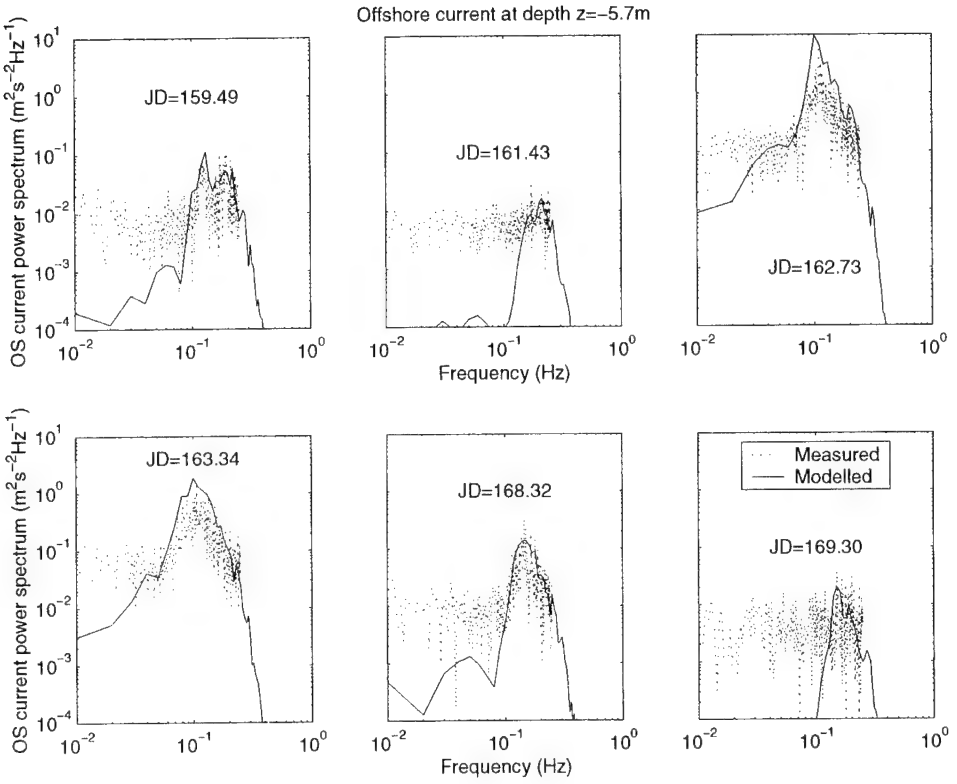

Figure 8 *Cross-shore current power spectra taken during different characteristic wave heights. The dashed curves are spectra of the measured current at depth $z = -5.7$ m and the solid curves are the spectra of modelled currents described by Eq. (12).*

timates of the dissipation of turbulent kinetic energy for varying mean currents and orbital velocities. Trowbridge and Agrawal (1995) used profiling laser Doppler velocimetry within the wave boundary layer to obtain the vertical structure of velocity. Their measurements also show a spectral slope of $-5/3$ indicating that the high frequency velocity variations are dominated by turbulence.

The model for the pressure variability according to (13) is compared by spectral analysis to measurements from the moored CTD for the six selected days. The CTD operated with a sampling frequency of 13 Hz for up to 1.5 h on selective days. The data were filtered with a two point average thus increasing the sampling interval to 0.15 s. The pressure signal was divided into M overlapping segments (the number of segments varied according to the length of the time series) with each segment having 1024 points. The pressure power spectrum was determined for each detrended segment and the segments were averaged to obtain one power spectrum.

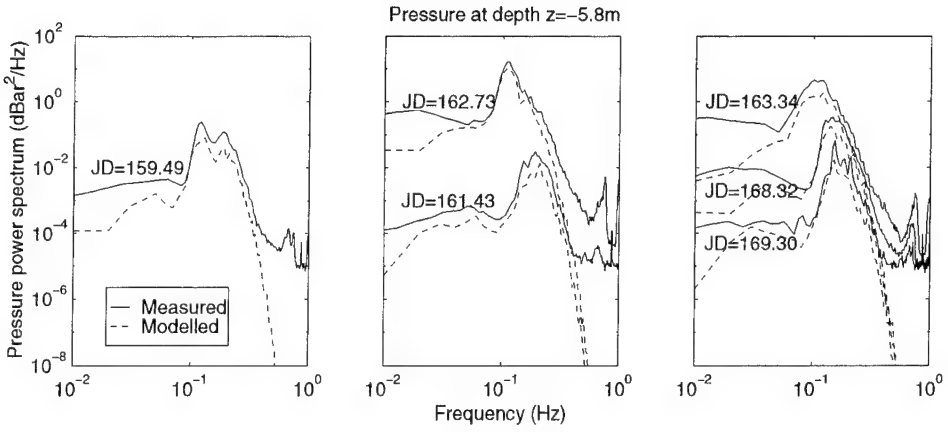

Figure 9 *Pressure power spectra taken during different characteristic wave heights. The solid curves are spectra of the measured pressure at depth $z = -5.8$ m and the dashed curves are the spectra from pressures modelled by Eq. (13).*

The results are shown in Figure 9. The modelled results for the pressure follows from generating a time series of $p(x = 0, z = -5.8m, t)$ sampled at the same rate as the wave rider buoy (1.28 Hz) and then computing the power spectra.

The comparison between modelled and measured is very good. The spectral peaks show the same characteristics and the levels are consistent thus confirming the linear summation of Stokes wave theory. At the peak of the storm (JD 162.73) the root-mean-square pressure fluctuation at 5.8 m depth is 0.6 m and a day later it reduces to 0.2 m. This variation in pressure will have an important effect on the sound speed during the storm, as will be shown.

The spectra of temperature, salinity and sound speed fluctuations were calculated in a similar way as was the measured pressure except that each segment length was 2048 points so that more low frequency information can be seen. Sound speed was calculated from the Mackenzie (1981) equation. The spectral results are shown in Figure 10 with model comparison. The spectra for vertical particle displacement (obtained in the same way as the pressure and horizontal orbital velocity) are multiplied by the gradients shown in Table 2 to match the spectral levels (dotted curves). Also shown in Table 2 is the sound speed gradient determined from (21) for comparison with the gradients determined from the spectral levels. The only time a significant difference arises is on Year Day 159.49 when there was strong stratification in temperature and salinity. From the thermistor chain a temperature gradient of 0.41 °C m^{-1} was measured during this time. On the other days it was measured as less than 0.1 °C m^{-1} which is subject to measurement uncertainty.

The power spectral results suggest frequency attenuation dependencies. For low fre-

Parameter	Julian Day					
	159.49	161.43	162.73	163.34	168.32	169.30
$\frac{dT}{dz}$ ($^oC\ m^{-1}$)	.54	.07	.01	.05	.03	.02
$\frac{dS}{dz}$ (psu m^{-1})	.63	.16	.02	.07	.22	.07
$\frac{1}{c_o}\frac{dc}{dz}$ ($\times 10^{-4}\ m^{-1}$)	7.85	1.64	0.53	1.31	1.64	0.65
$a\frac{dT}{dz} + b\frac{dS}{dz}$ ($\times 10^{-4}\ m^{-1}$)	13.78	2.36	0.35	1.37	2.20	0.81

Table 2 *Gradients of temperature, salinity and sound speed determined by comparing measured spectral data to the models described by (18), (19), (20), and (21).*

quencies (to the left of the particle displacement effect, $f < 0.1$ Hz) the data seem to show a $-5/3$ power law (dashed curves) during times when there are strong vertical displacements in the presence of stratification. This power law suggests an inertial sub range for the scalar variability according to Kolmogorov theory (Hinze, 1959). It is hypothesized that wave-current interaction is the driving force for the turbulence occurring at frequencies lower than the orbital motions. For higher frequencies (to the right of the particle displacement effect, $f > 0.1$ Hz) the data show a slope dependence of approximately $f^{-3.5}$ (dashed dot curves) indicating that turbulence is not dominating the scalar variance at these frequencies. It is not clear what physical process causes this characteristic which appears to be consistent. During calm conditions when the significant wave heights were less than 0.5 m, the power laws break down (see for example on Year Days 161.43 and 169.3 for all variables).

For the sound speed spectra it is interesting to note that on Year Day 162.73 (during the storm event) the spectral peak is dominated by pressure effects as during this time no significant peak associated with surface wave effects can be seen in the temperature and salinity spectra. Also, the gradient of temperature and salinity as measured by the spectral technique, is low. On Year Day 168.32 the sound speed is dominated by large variations in salinity (≈ 1 psu) caused by advection as precipitation and Magra river transport were negligible. The corresponding salinity gradient during this time is 0.22 psu m^{-1}. On other days temperature and salinity variations give rise to the observed sound speed variations.

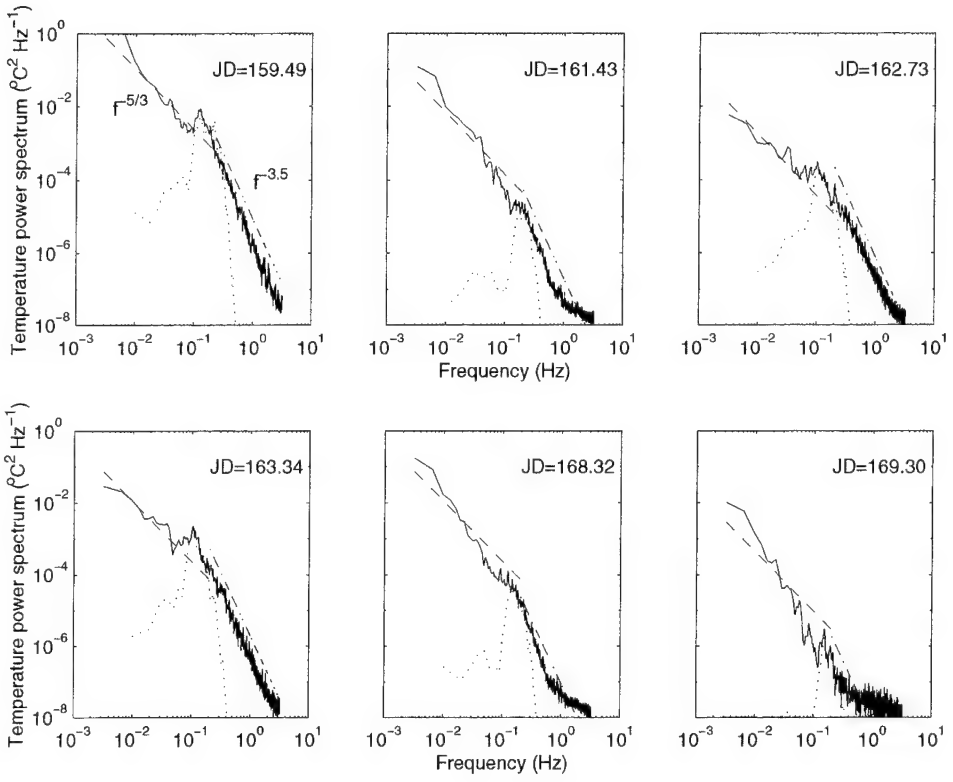

(a)

Figure 10 *Power spectra for (a) temperature, (b) salinity and (c) sound speed together with the spectra of vertical particle displacement scaled by the gradients in Table 2 (dotted curve). Slopes showing a $-5/3$ power low (dashed curve) and a -3.5 power law (dashed-dot curve) are also shown for comparison.*

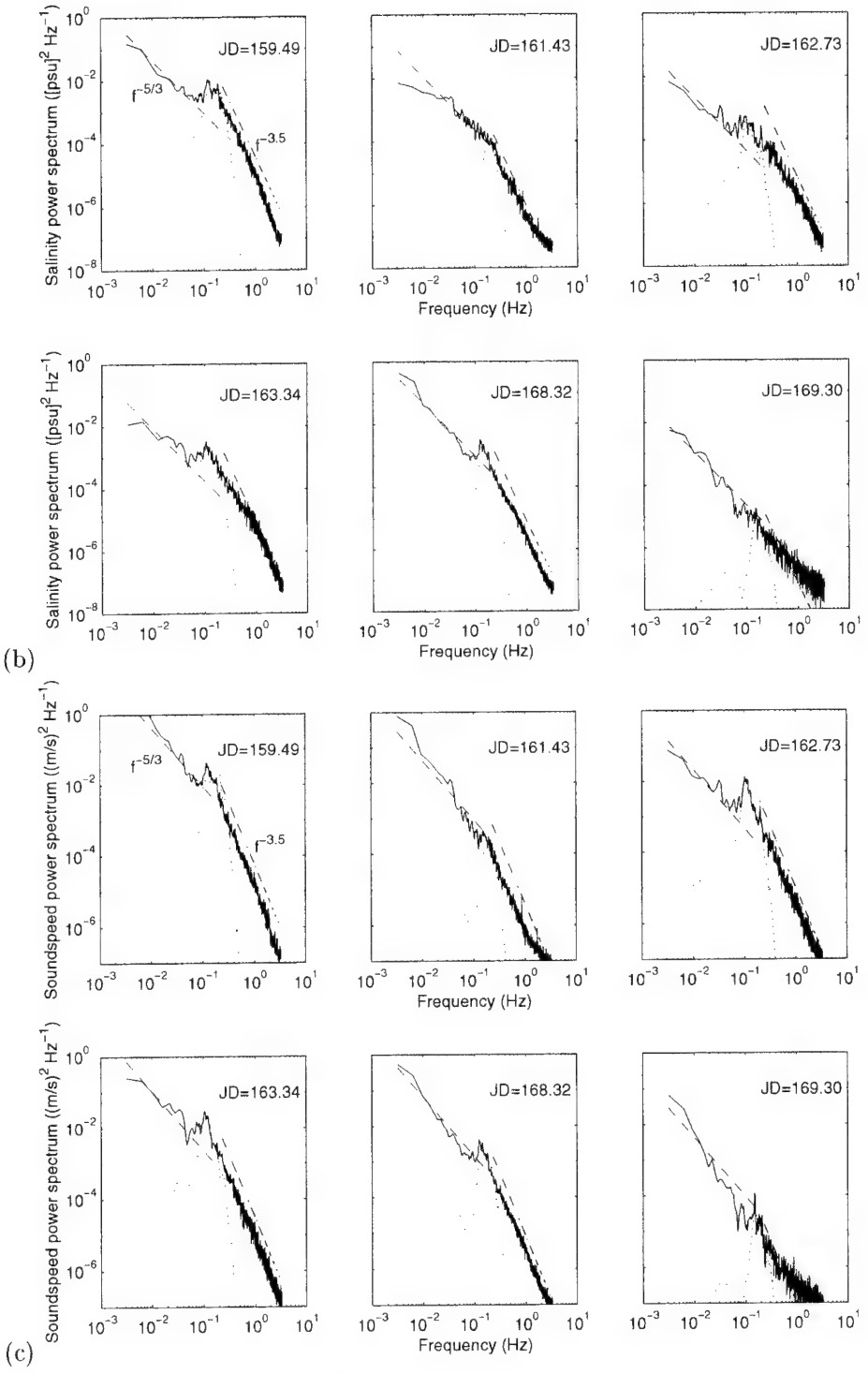

Figure 10 *(continued).*

5
Conclusions

During heavy rainfall (precipitation exceeding 5 mm) there was a corresponding salinity decrease of approximately 0.5-1 psu at 5.8 m depth. Some of these changes could also be the result of advection from wind-driven currents. Analysis of wind data showed that the cross-shore winds exhibit 24 h periodicity associated with land/sea breezes as a result of land cooling and heating respectively. The 24 h periodicity of the cross-shore winds was reflected in the temperature (and salinity) variations leading to the conclusion that advection by wind and precipitation were the primary cause of the large low frequency variations.

Sea surface wave data were characteristic of Mediterranean swell (mean period 4 s and significant wave heights less than 1 m), except during a storm, when significant wave heights exceeded 3 m and therefore the theory of Stokes finite amplitude waves and linear theory were used to model particle motion, pressure, temperature/salinity and sound speed variations. Observations and models were compared on six different days: a local storm event, a calm period, during the peak of a major storm, the post-storm stage, during swell-dominated seas and finally when the sea was calm again.

The velocity field showed current oscillations characteristic of a wave boundary layer. Tidal and wind-driven currents were small compared to the magnitude of the orbital velocities. The wave Reynolds number during active sea states was of the order 3×10^6 indicating that the wave boundary layer undergoes fully developed turbulence. Noise in the ADCP measurement limited the velocity fine scale measurement to orbital velocities during times when the significant wave height exceeded 0.5 m and limited its comparison to modelled orbital velocity spectra.

The temperature/salinity and hence sound speed variations showed that when the orbital particle motions were strong, there was a low frequency spectral power law of $f^{-5/3}$ to the left of the surface wave peak and a high frequency spectral power attenuation of $f^{-3.5}$ to the right. The $-5/3$ power law dependence corresponds to the inertial sub range for a fully developed turbulent wave boundary layer. As this occurs at frequencies lower than the orbital motions, it is hypothesized that the driving force for the turbulence is wave-current interaction.

6

Acknowledgements

The authors wish to thank the technical staff involved in the deployment, maintenance and recovery of oceanographic instrumentation, in particular R. Della Maggiore, R. Stoner and the captain and crew of T-Boat *Manning*. Thanks to E. Nacini for his assistance in obtaining the precipitation and river transport measurements.

References

Bowden, K. (1983). *Physical Oceanography of Coastal Waters.* Ellis Horwood Ltd.

Datawell (1996). WAREC - PC Software, 3-D WAREC. Technical report, Datawell bv, The Netherlands.

Donelan, M., Hamilton, J., and Hui, W. (1985). Directional spectra of wind-generated waves. *Phil. Trans. R. Soc. Lond.*, 315:509–562.

Edson, J., Fairall, C., Mestayer, P., and Larsen, S. (1991). A study of the inertial-dissipation method for computing air-sea fluxes. *J. Geophys. Res.*, 96:10689–10711.

Gemmrich, J. and Farmer, D. (1999). Near-surface turbulence and thermal structure in a wind-driven sea. *J. Phys. Oceanogr.*, 29:480–499.

Grant, W. and Madsen, O. (1979). Combined wave and current interaction with a rough bottom. *J. Geophys. Res.*, 84:1797–1808.

Gross, T., Williams, A., and Terray, E. (1994). Bottom boundary layer spectral dissipation estimates in the presence of wave motions. *Cont. Shelf Res.*, 14:1239–1256.

Hinze, J. (1959). *Turbulence: An Introduction to its Mechanism and Theory.* McGraw-Hill Series in Mechanical Engineering.

Ippen, A. (1966). *Estuary and Coastline Hydrodynamics.* McGraw-Hill Book Comp. Inc.

Lamb, H. (1932). *Hydrodynamics.* Dover Publications, N.Y.

Lumley, J. and Terray, E. (1983). Kinematics of turbulence convected by a random wave field. *J. Phys. Oceanogr.*, 13:2000–2007.

Mackenzie, K. (1981). Nine-term equation for sound speed in the oceans. *J. Acoust. Soc. Am.*, 70:807–812.

Neumann, G. and Pierson, W. (1966). *Principles of Physical Oceanography.* Prentice-Hall Inc.

Phillips, O. (1985). Spectral and statistical properties of the equilibrium range in wind-generated gravity waves. *J. Fluid Mech.*, 156:505–531.

Press, W., Flannery, B., Teukolsky, S., and Vetterling, W. (1986). Fourier and spectral applications. In *Numerical Recipes - The Art of Scientific Computing*, chapter 13. Cambridge University Press, 2nd edition.

Shemdin, O., Hasselmann, K., Hsiao, S., and Herterich, K. (1978). Nonlinear and linear bottom interaction effects in shallow water. In Favre, A. and Hasselman, K., editors, *Proceedings of the NATO conference on Turbulent Fluxes through the Sea Surface, Wave Dynamics and Prediction*, Marseille, France, Sept. 12-16, 1977. Plenum Press, NY.

Trowbridge, J. and Agrawal, Y. (1995). Glimpses of a wave boundary layer. *J. Geophys. Res.*, 100:20729–20743.

Wiberg, P. (1995). A theoretical investigation of boundary layer flow and bottom shear stress for smooth, transitional, and rough flow under waves. *J. Geophys. Res.*, 100:22667–22679.

Document Data Sheet

Security Classification		Project No.
UNCLASSIFIED		03-D
Document Serial No.	**Date of Issue**	**Total Pages**
SR-322	March 2000	35 pp.

Author(s)

Di Iorio, D., Bergem, O., Pace, N.

Title

Effects of the atmosphere and sea-surface waves on current and temperature/salinity variations in a shallow water environment.

Abstract

A shallow water experiment (d = 10 m) was carried out to measure the contribution of wind, precipitation and sea surface wave effects on current, pressure and temperature/salinity variations. It is found that during heavy rainfall (precipitation exceeding 5 mm) , there is a corresponding salinity decrease of approximately 1 psu at 5.8 m depth. Analysis of wind data shows that the cross-shore winds exhibit 24 h periodicity associated with land/sea breezes as a result of land cooling and heating. The 24 h periodicity of cross-shore winds is reflected in temperature and salinity variations leading to the conclusion that advection by wind is the primary cause of low frequency variations. Sea surface wave data show predominantly Mediterranean swell (mean period 4 s and significant wave heights less than 1 m). During the passage of a storm, significant wave heights exceeded 3 m and so the theory of Stokes finite amplitude waves in conjunction with linear theory is used to model particle motion, pressure, temperature/salinity and sound speed variations. Observations and models are compared for six different days and conditions: a local storm event, a calm period, during the peak of a major storm, the post-storm stage, during swell-dominated seas and finally when the sea was calm again. The velocity field shows current oscillations characteristic of a wave boundary layer. The temperature/salinity and hence sound speed variations show that when the orbital particle motions are strong, there is a low frequency spectral power law of $f^{-5/3}$ to the left of the surface wave peak and a high frequency spectral power attenuation of approximately $f^{-3.5}$ to the right.

Keywords

Stokes waves – wave boundary layer – turbulence – Mediterranean Sea

Issuing Organization

North Atlantic Treaty Organization
SACLANT Undersea Research Centre
Viale San Bartolomeo 400, 19138 La Spezia, Italy

[From N. America: SACLANTCEN (New York) APO AE 09613]

Tel: +39 0187 527 361
Fax:+39 0187 527 700

E-mail: library@saclantc.nato.int

The SACLANT Undersea Research Centre provides the Supreme Allied Commander Atlantic (SACLANT) with scientific and technical assistance under the terms of its NATO charter, which entered into force on 1 February 1963. Without prejudice to this main task - and under the policy direction of SACLANT - the Centre also renders scientific and technical assistance to the individual NATO nations.

SACLANT Undersea Research Centre
Viale San Bartolomeo 400
19138 San Bartolomeo (SP), Italy

tel: +39 0187 527 (1) or extension
fax: +39 0187 527 700

e-mail: library@saclantc.nato.int

NORTH ATLANTIC TREATY ORGANIZATION